PLOS ONE

RESEARCH ARTICLE

^{18}F-FDG-PET/MRI in the diagnostic work-up of limbic encephalitis

Cornelius Deuschl[1]*, Theodor Rüber[2], Leon Ernst[2], Wolfgang P. Fendler[3], Julian Kirchner[4], Christoph Mönninghoff[1,5], Ken Herrmann[3], Carlos M. Quesada[6], Michael Forsting[1], Christian E. Elger[2], Lale Umutlu[1]

1 Institute for Diagnostic and Interventional Radiology and Neuroradiology, University Hospital Essen, University of Duisburg-Essen, Essen, Germany, **2** Department of Epileptology, University of Bonn, Bonn, Germany, **3** Department of Nuclear Medicine, University Hospital Essen, University of Duisburg-Essen, Essen, Germany, **4** Department of Diagnostic and Interventional Radiology, University Duesseldorf, Medical Faculty, Duesseldorf, Germany, **5** Clinic for Neuroradiology, Clemenshospital Muenster, Muenster, Germany, **6** Department of Neurology, University Hospital Essen, University of Duisburg-Essen, Essen, Germany

* cornelius.deuschl@uk-essen.de

Citation: Deuschl C, Rüber T, Ernst L, Fendler WP, Kirchner J, Mönninghoff C, et al. (2020) ^{18}F-FDG-PET/MRI in the diagnostic work-up of limbic encephalitis. PLoS ONE 15(1): e0227906. https://doi.org/10.1371/journal.pone.0227906

Editor: Giorgio Treglia, Ente Ospedaliero Cantonale, SWITZERLAND

Received: November 26, 2019

Accepted: January 2, 2020

Published: January 17, 2020

Data Availability Statement: All relevant data are within the manuscript.

Funding: The authors received no specific funding for this work.

Competing interests: The authors have declared that no competing interests exist.

Abstract

Introduction

Limbic encephalitis (LE) is an immune-related, sometimes paraneoplastic process of the central nervous system. Initial diagnosis and treatment are based on the clinical presentation as well as antibody profiles and MRI. This study investigated the diagnostic value of integrated ^{18}F-FDG-PET/MRI in the diagnostic work-up of patients with LE for a cerebral and whole-body imaging concept.

Material and methods

Twenty patients with suspected LE were enrolled in this prospective study. All patients underwent a dedicated PET/MRI protocol of the brain as well as the whole-body. Two neuroradiologists, one body radiologist and one nuclear medicine physician performed blinded consensus readings of each corresponding MRI and PET/MRI dataset of the brain and whole-body. Diagnostic confidence was evaluated on a Likert scale.

Results

Based on integrated PET/MRI 19 / 20 patients were found to show morphologic and / or metabolic changes indicative of LE, whereas sole MRI enabled correct identification in 16 / 20 patients. Three patients with negative MRI showed metabolic changes of the limbic system or extra-limbic regions, shifting the diagnosis from (negative) MRI to positive for LE in PET/MRI. Whole-body staging revealed suspected lesions in 2/20 patients, identified by MRI and PET, one confirmed as malignant and one false positive. Diagnostic confidence for cerebral and whole-body imaging reached higher scores for PET/MRI (cerebral: 2.7 and whole body: 4.8) compared to MRI alone (cerebral: 2.4 and whole body: 4.5).

Conclusion

LE diagnosis remains challenging for imaging as it shows only subtle imaging findings in most patients. Nevertheless, based on the simultaneous and combined analysis of morphologic and metabolic data, integrated PET/MRI may enable a dual platform for improved diagnostic confidence and overall detection of LE as well as whole-body imaging for exclusion of paraneoplastic LE.

Introduction

Limbic encephalitis (LE) is an autoimmune-mediated syndrome, most commonly caused by either infectious or autoimmune diseases. In a minority of cases, LE is caused by an (undetected) tumor in the patients´ body which activates the immune system, also referred to as "paraneoplastic limbic encephalitis". Diagnosis remains challenging due to its unspecific clinical presentation with loss of short-term memory, mental status changes or general psychiatric symptoms, as not all patients feature temporal lobe seizures [1]. Positive autoimmune antibodies in the cerebrospinal fluid is a common finding in patients with LE and is considered an important criterion for diagnosing LE. In the majority of cases imaging findings in magnetic resonance imaging (MRI) comprise subtle changes, mostly characterized by T2 hyperintensities and volume alterations in mesial temporal structures, making a correct, standardized diagnosis difficult [2, 3]. These volume alterations are typically characterized by increase or loss of hippocampal or amygdala volume [4, 5]. Apart from MRI, ^{18}F-fluorodeoxyglucose positron emission tomography (^{18}F-FDG-PET) has been shown to facilitate the visualization of changes of the glucose metabolism in mesial temporal structures as well as extra limbic regions and hence support the correct diagnosis of LE [6]. Metabolic information derived from ^{18}F-FDG-PET has been shown particularly helpful in patients with indifferent or negative MRI [7, 8]. Aside from these promising results, to date, studies mostly focused either on sole morphological analysis of MRI or sole metabolic analysis of PET data for diagnosis of LE, lacking dedicated studies on the diagnostic value of integrated ^{18}F-FDG-PET/MRI. The introduction of integrated PET/MRI scanners has facilitated a new platform for simultaneously acquired and co-registered morphologic and metabolic data, which has been widely used for numerous application fields.

Hence, the aim of this study was to evaluate the diagnostic value of hybrid ^{18}F-FDG-PET/MRI for cerebral evaluation and whole-body imaging to diagnose LE and detect / exclude paraneoplastic LE.

Material and methods

Patients and inclusion criteria

The study was conducted in accordance with all guidelines set forth by the approving institutional review board. The study was approved by the ethics committee of the University Duisburg-Essen. All patients gave written informed consent before undergoing ^{18}F-FDG PET/MRI. Twenty patients (mean age: 38 years, range: 18–76 years, 15 female, 5 male) with suspected LE were included in this prospective study over the time course of 23 months (Table 1).

Positive antibody profiles were detected in 13 patients (8 with antiglutamic acid decarboxylase (GAD) antibodys, two patients with positive leucine-rich glioma-inactivated 1 (LGI1), two

Table 1. Patient data, antibodies, clinical findings.

Pat.	Sex	Age	Antibody	EEG	Limbic symptoms
1	f	32	-	left temp.	+
2	f	19	-	left temp.	+
3	m	75	LGI1 +	right temp.	+
4	m	26	LGI1 +	-	+
5	m	33	-	left temp.	+
6	f	21	Ma2/Ta+	left temp.	+
7	f	31	GAD+	left temp.	+
8	m	45	GAD+	-	+
9	f	29	GAD+	left temp.	+
10	f	30	GAD+	bilat.temp.	+
11	f	39	GAD+	bilat.temp.	+
12	f	37	-	right temp.	+
13	f	32	GAD+	left temp.	+
14	m	59	GAD +	right temp.	+
15	f	20	-	bilat.temp.	+
16	f	32	CV2+	left temp.	+
17	f	44	CV2+	-	+
18	f	76	-	right temp.	+
19	f	62	GAD+	-	+
20	f	18	-	bilat.temp.	+

https://doi.org/10.1371/journal.pone.0227906.t001

patients for anti-CV2 (CV2) and one patient for anti-Ma2/Ta (Ma2/Ta). 16 patients showed pathologic EEG findings and all patients showed positive limbic symptoms.

Suspected LE was diagnosed by the treating physician based on the German Guidelines on immune related cerebral disease [9]. All patients had suffered from at least one limbic symptom within the last 5 years (e.g. dysfunction of the episodic memory, seizures with temporal semiology, or psychiatric symptoms with affect lability), that initially showed a subacute onset with rapid progression. Moreover at least one of these parameters: (1) positive autoimmune antibodies in the cerebrospinal fluid or (2) brain abnormalities of the medial temporal lobe on T2-weighted MRI restricted to one or both medial temporal lobes (Table 1). Reasonable exclusion of alternate causes. Moreover, the treating physician used all information including electroencephalogram (EEG) findings and therapy response on anti-autoimmune treatment for diagnosis [10].

Brain PET/MRI

PET/MR Imaging was performed on an integrated 3T hybrid PET/MRI system (Biograph mMR, Siemens Healthcare, Erlangen, Germany). Prior to the examination patients were prepared in accordance to the EANM guidelines for PET brain imaging using ^{18}F-FDG [11]. Image acquisition started 60 min intravenous after injection of ^{18}F-FDG (mean ± SE, 236.5 MBq; ± 10,04 MBq). PET imaging of the head was performed in one bed position (axial field of view 25.8 cm) with an acquisition time of 20 min while simultaneously acquiring the MRI sequences. PET data were reconstructed in 3D mode using ordinary Poisson ordered subsets expectation maximization with 3 iterations and 21 subsets and a Gaussian filter with 4 mm FWHM and 344 × 344 voxels. For attenuation correction Dixon sequence-based AC was used.

Table 2. Sequence parameters for the diagnostic MR sequences used in PET/MRI.

Name	Region	Orientation	TR (ms)	TE (ms)	Matrix size	Slice thickness (mm)
3D-T1-MPRAGE	Brain	sagittal	1670	2.56	0/320/310/0	0.8
3D-FLAIR	Brain	sagittal	5000	284	0/256/248/0	1
SWI	Brain	transversal	26	20	0/256/187/0	2
STIR TSE	Brain	coronal	5930	25	0/512/384/0	2
T2-TSE	Brain	temporal	6000	96	0/256/187/0	4
T2-TSE	Brain	ACPC	6000	96	0/512/384/0	4
ce 3D-MPRAGE	Brain	sagittal	1790	2.67	0/512/256/0	1
VIBE	Whole-body	coronal	3.64	1.49	512/0/0/230	3.5
DWI	Whole-body	transversal	6500	56	160/0/0/90	5
HASTE	Whole-body	transversal	1500	97	320/0/0/194	7
ce VIBE	Whole-body	transversal	3.64	1.49	512/0/0/230	3.5

https://doi.org/10.1371/journal.pone.0227906.t002

MR imaging was performed simultaneously to PET data acquisition, utilizing a dedicated 16-channel head and neck radiofrequency coil. The MRI protocol comprised the following sequences, detailed information is displayed in Table 2:

1. a high-resolution three-dimensional (3D) magnetization-prepared rapid acquisition with gradient echo (3D-T1-MPRAGE) sequence
2. a three-dimensional (3D) fluid-attenuated inversion recovery (3D-FLAIR) sequence
3. a transversal susceptibility-weighted imaging [12] sequence
4. a coronal Short tau inversion recovery (STIR) sequence
5. a temporal and an anterior commissure—posterior commissure orientation (ACPC) T2 weighted turbo spinecho sequence
6. a contrast-enhanced high-resolution three-dimensional (3D) magnetization-prepared rapid acquisition with gradient echo (ce3D-T1-MPRAGE) sequence (0.2 mmol/1 kg body weight of contrast agent (Dotarem®, Guerbet, Sulzbach/Taunus, Germany)).

Whole-body PET/MRI

After the brain examination whole-body imaging was obtained in 4–5 bed positions (from skull-base to mid-thighs) with a PET acquisition time of 4 min / bed position. PET image reconstruction was performed subsequently utilizing the OSEM algorithm, 3 iterations and 21 subsets, a Gaussian filter with 4 mm, FWHM and a 344x344 image matrix. For MRI data acquisition a dedicated mMR head-and-neck radiofrequency (RF) coil and RF body array surface coils were used [13]. The total scan duration of the whole-body protocol amounted to 27.8 ±3.7 min and comprised the following sequences, detailed information is displayed in Table 2:

1. a 3-dimensional volume interpolated breath-hold examination (VIBE) sequence for Dixon-based attenuation correction
2. a diffusion-weighted (DWI) echo-planar imaging (EPI) sequence
3. a 2-dimensional half Fourier acquisition single-shot turbo spin echo (HASTE) sequence
4. a post-contrast 3-dimensional fat-saturated VIBE sequence.

Image analysis

Two board certified neuroradiologists, one board certified body radiologist and one board certified nuclear medicine physician performed consensus readings of the MRI, PET and fused PET/MRI datasets of the brain and whole-body. MRI and PET/MRI were assessed independently in two sessions with a break of 4 weeks to avoid recognition bias. Readings were performed on a PACS workstation (Centricity Radiology R1000, GE Healthcare, IL, USA) as well as on a dedicated viewing software for integrated imaging (Scenium Software, Syngo.via; Siemens Healthcare, Erlangen, Germany). The readers were blinded for the patients´ final diagnosis but had access to all relevant clinical information like EEG, clinical presentation, antibody status.

Brain imaging. All datasets were visually interpreted. MR-criteria indicative of a limbic encephalitis include (1) T2 hyperintensity of the amygdala, of the hippocampus and/ or insula and (2) volume alterations of the mesial temporal structures [2, 14]. Additionally, PET images were visually interpreted and analysed for any hypo- or hypermetabolism of the limbic system. Aside from changes in the limbic system, any extra-limbic metabolic changes indicative / potentially associated to LE were noted as well. Furthermore, the readers used stereotactic surface projection for analysis (SSP, Syngovia, Siemens Healthcare, Erlangen, Germany). SSP analysis was performed based on a software implemented matched reference cohort scanned on a Biograph PET/CT supplied by SyngoVia.

In addition, the readers indicated their diagnostic confidence on a Likert scale (1-not at all confident, 2-not very confident, 3-neutral, 4-confident, 5-very confident) for MRI alone, PET alone and integrated PET/MRI for brain imaging. Data are presented as mean +/- standard deviation. Descriptive analysis was used to evaluate the resulting scores.

Whole-body imaging. In accordance with previous publications the following criteria were considered indicative of malignancy of lesions in the whole-body datasets: (1) lesion shape, (2) local invasiveness, (3) central necrosis, (4) increased contrast enhancement, and (5) diffusion restriction [15]. Lymph nodes with a short axis diameter $>$ 10 mm, spherical configuration and increased contrast enhancement were classified as nodal metastases. In accordance with previous publications visually detectable focal ^{18}F-FDG uptake above the surrounding background was considered as a sign of malignancy on PET / PET/MRI [15].

Results

Hybrid ^{18}F-FDG-PET/MRI was successfully completed in all 20 examinations and no relevant artifacts (leading to an exclusion of datasets) were detected.

Brain imaging

Morphologic imaging. Two board certified neuroradiologists performed a consensus reading of the MRI datasets and reported changes of the limbic system in 16/20 patients (80%) (Table 3).

Out of these 16 patients, 8 showed unilateral enlargement and/or T2/FLAIR signal increase of the amygdala (Figs 1A, 1B, 2A and 2B) and the hippocampus.

7 patients demonstrated bilateral swelling and T2/FLAIR signal increase of the amygdala and/or hippocampus. In one patient hippocampal sclerosis was detected based on a reduced hippocampal volume with increased T2/FLAIR signal. In 4/20 patients no pathologic changes were found on MRI.

Hybrid imaging. One board certified nuclear medicine physician and two board certified neuroradiologists analyzed the PET/MRI datasets of the brain in a consensus reading. The evaluation of hybrid imaging revealed corresponding morphologic and or metabolic changes

Table 3. Results of cerebral PET/MRI.

Pat.	Antibody	MRI	MRI Finding	PET	PET Finding	Z-Scores *
1	-	+	Amygdala and hippocampus swelling and T2 hyperintensity left	+	Bifrontal hypometabolsim	1.1; 1.2 // 2; 1.9 // -0.5; 0.7 // 1.4; 1.9 // 1.6; 1.6
2	-	+	Hippocampal sclerosis left	+	Hypometabolism left amygdala	-0.1; -1.8 // 0.8; -0.1 // -2.5; -3.8 // -0.6; -1.6// 0; 0.1
3	LGI1 +	+	Bilateral amygdala swelling and T2 hyperintensity	+	Hypermetabolism right amygdala and hippocampus & bitemporal, -and biparietal and hypometabolism	4.9; 2.4 // 3.3; 1.8 // -1.1; -0.9 // -0.3; -0.8 // 1.3; 0.7
4	LGI1 +	-	-	-	-	-1.2; 0.2 // -0.3; -0.4 // -2.4; -2 // -1.1; -1.2 // 0.2; 0
5	-	-	-	+	Hypometabolism left amygdala	1; -2// 0.1; -0.4 // -0.9; -1.7 // -0.4; -0.5 // -1; -0.8
6	Ma2/Ta+	+	Amygdala swelling an T2 hyperintensity left	+	Hypometabolism left amygdala, hippocampus & bitemporal and biparietal hypometabolism	0.2; -1.8 // 0.4; -0.2 // -1.5; -3.8 // -0.6; -1.3 // 0.1; 0
7	GAD+	-	-	+	Hypometabolism left amygdala + bitemporal and biparietal lobe hypometabolism	-1.2; -2.5 // -0.7; -0.9 // -3.3; -2.9 // -2.3; -1.8 // 1.4; 1.3
8	GAD+	+	Amygdala and hippocampus swelling an T2 hyperintensity left	-	-	-0.4; -0.5 // -0.9; -2.3 // 1.4; 1.9 // 1.3; 1.8 // -2.1; -1.6
9	GAD+	+	Amygdala swelling and T2 hyperintensity left	-	-	0.2; 0.3 // 0.2; -0.4 // 1.1; 0.5 // 1.3; 0.8 // -0.7; -1.5
10	GAD+	+	Amygdala swelling and T2 hyperintensity bilateral	-	-	0.5; -0.4 // -2.3; -0.9 // 1.9; 1.4 // 2.8; 1.3 // -2.1; -1.4
11	GAD+	+	Amygdala swelling and T2 hyperintensity left	-	-	1.8; 1.1 // 1; 1.3 // 0; -0.3 // -0.4; -0.4 // 1; 0.8
12	-	-	-	+	Bitemporal and biparietal hypometabolism	1.1; 0.5 // 1.1; 1.5 // -0.9; -0.7 // 0.4; 0.6 // 1.1; 1.1
13	GAD+	+	Hippocampus and amygdala T2 hyperintensity bilateral	-	-	-0.5; 0 // -0.9; -0.1 // -2.2; -1.9 // -2; -1.2 // -1; -0.5
14	GAD +	+	Hippocampus swelling and amygdala T2 hyperintensity right	+	Hypometabolism right amygdala	-1.1; 1.2 // 0.9; 1.6 // -0.1; -0.5 // 0.4; -0.5 // 0.5; 0.6
15	-	+	Hippocampus and amygdala T2 hyperintensity bilateral	-	-	0.7; 0 // -0.7; -0.3 // -0.8; -1.7 // -0.3; -0.8 // -1.3; -1.1
16	CV2+	+	Hippocampus and amygdala T2 hyperintensity bilateral	-	-	0.2; -0.1 // -0.5; 0.4 // -3.4; -2 // -1.1; 0 // -0.4; -0.1
17	CV2+	+	Hippocampus and amygdala T2 hyperintensity bilateral	-	-	0.6; 0.2 // -0.6; 0.5 // 1,1; -0.6 // 0.6; 0 // 0.6; 1.2
18	-	+	Hippocampus and temporal lobe swelling and T2 hyperintensity right	+	Hypometabolism right amygdala and hippocampus & hypometabolism right parietal lobe	-1.2; -0.8 // 0.5; -0,6 // -0.6; -1.1 // 0; 0.6 // 1.2; 0.6
19	GAD+	+	Hippocampus and amygdala swelling and T2 hyperintensity bilateral	+	Hypometabolism right amygdala	-1.6; 0.2// -0.6; 0.5// -1.1; -0.6 // 0; 0.6 // 0.6; 1.2
20	-	+	Amygdala swelling and T2 hyperintensity left	-	-	0.1; 1 // 1.2; 1.1 // -2; -1.6 // -2.4; -2.7 // -1.6; -1.1

*Z-Scores from detailed SSP analysis displayed as following: Amygdala right; amygdala left // hippocampus right; hippocampus left // temporal pole: superior temporal gyrus right; temporal pole: superior temporal gyrus left // temporal pole: middle temporal gyrus right; temporal pole: middle temporal gyrus left // thalamus right; thalamus left.

https://doi.org/10.1371/journal.pone.0227906.t003

of the limbic system and extra limbic areas in 19/20 patients (95%). Out of these 19 patients, 16 patients showed morphologic changes, whereas 7 of these patients showed additional metabolic changes (three with changes of the limbic system, three with changes of the limbic system and additional extra-limbic involvement and one patient with isolated extra-limbic hypometabolism) (Figs 1 and 2). Three of the 20 patients showed negative MRI but positive PET, one revealing metabolic changes of the limbic system, one with hypometabolism of the limbic system and the extra-limbic structures and one patient with extra-limbic involvement, changing

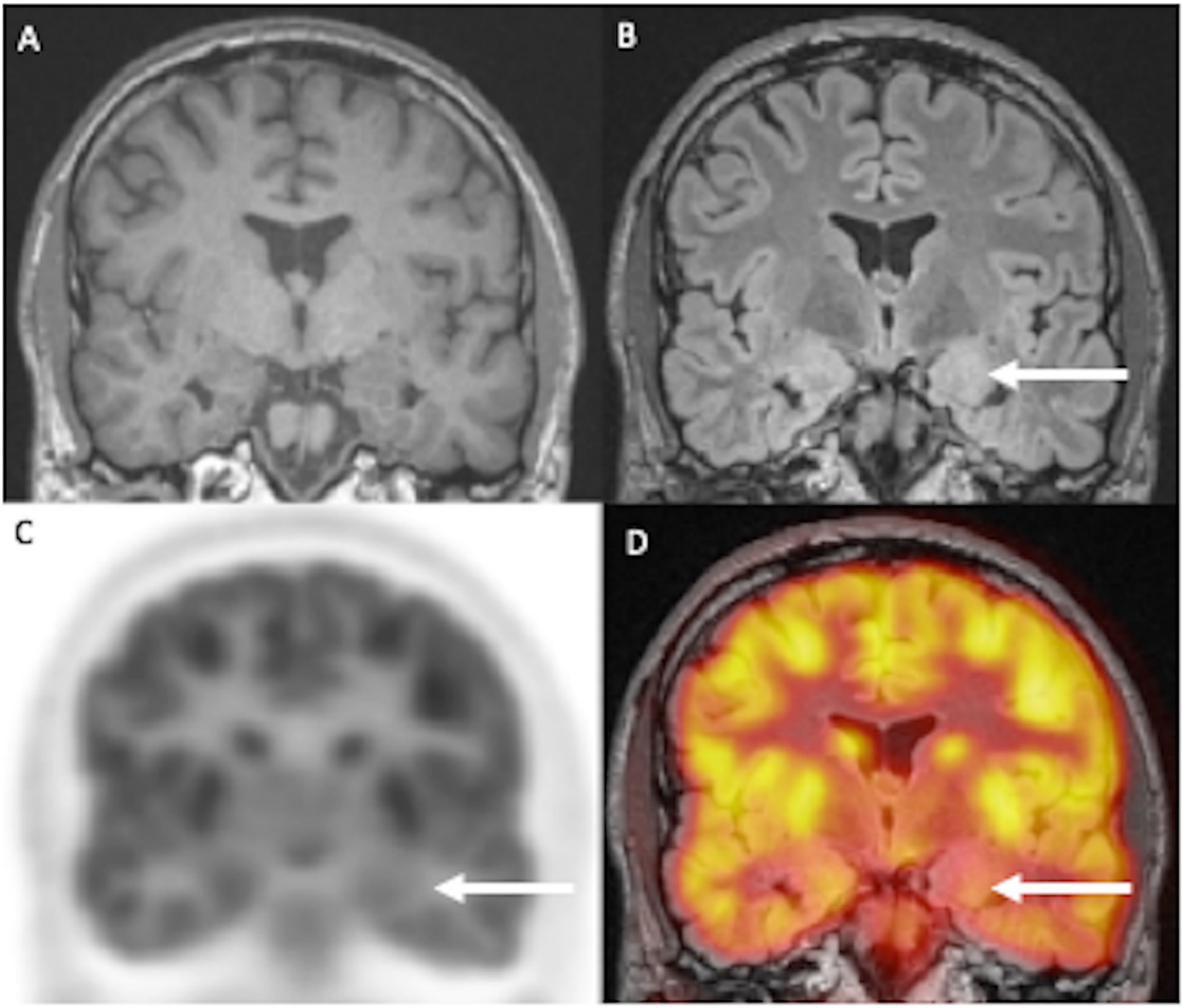

Fig 1. 21-year old female patient with swelling and FLAIR hyperintensity of the left amygdala (A, B). PET shows corresponding glucose hypometabolism (C, D).

https://doi.org/10.1371/journal.pone.0227906.g001

the diagnosis from negative MRI to suspected LE in hybrid imaging. Another patient did not show any pathological changes in MRI or PET (Table 3).

Diagnostic confidence. Diagnostic confidence on a five-point Likert scale reached higher values for hybrid PET/MRI with 2.7 when compared to sole MRI with 2.4.

Whole-body imaging

Morphologic imaging. One board certified body radiologist and a nuclear medicine specialist performed a consensus reading of the whole-body MRI sequences. In 2/20 patients suspicious lesions were detected (Table 4).

In one patient rectal cancer was diagnosed on MRI and confirmed by histopathology (Fig 3).

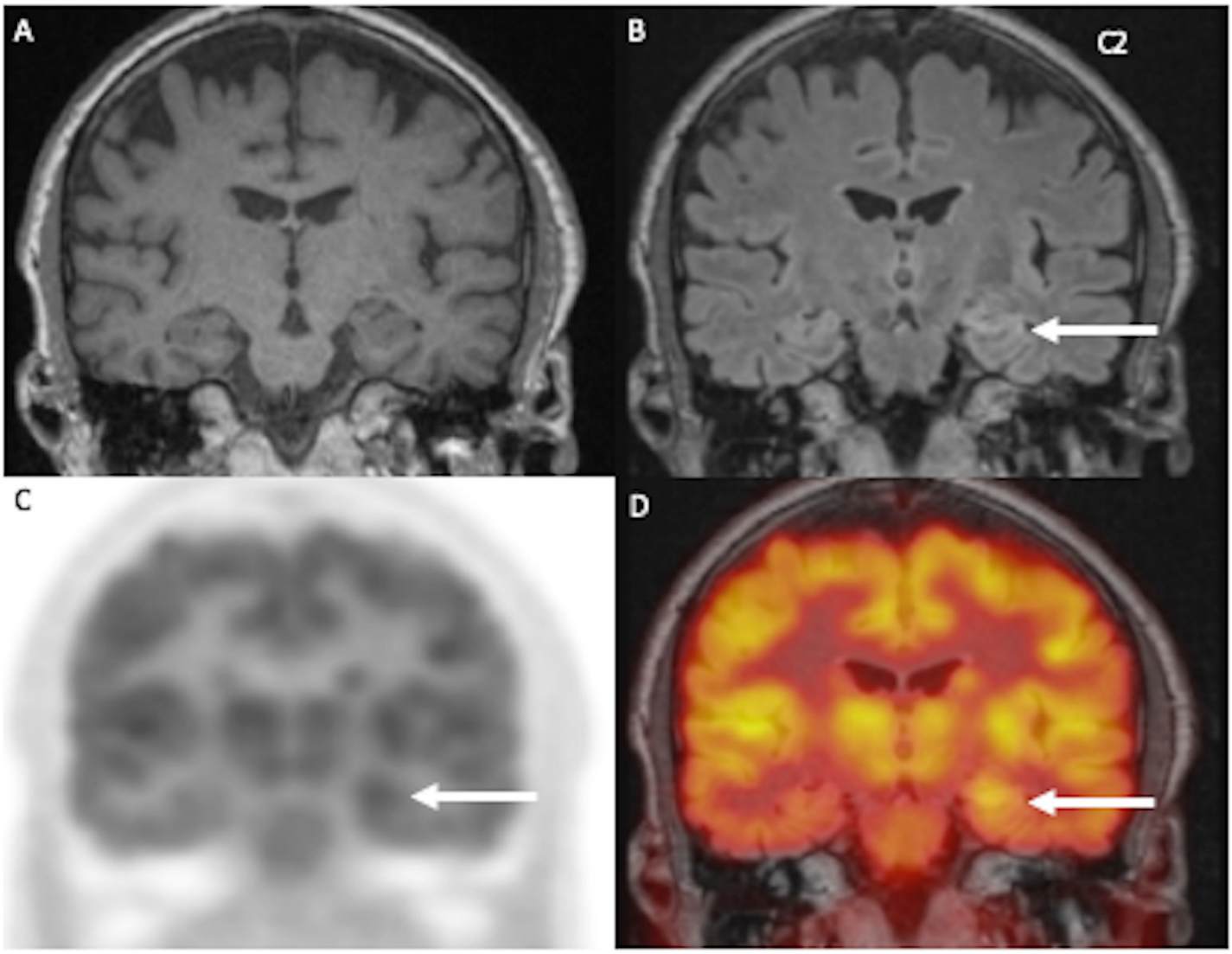

Fig 2. 75-year old patient with left sided enlargement of the hippocampus on T1 (A) and dull FLAIR-hyperintensity (B). Corresponding glucose hypermetabolism of the left hippocampus and amygdala can be detected on FDG-PET (C) and fusion with FLAIRw (D).

https://doi.org/10.1371/journal.pone.0227906.g002

In one patient suspicious bilateral subscapular lesions were described on MRI with mild glucose uptake (Fig 4).

Further clinical diagnostics showed no evidence of oncological disease in this patient, making an elastofibroma dorsi the most likely diagnosis [16].

Hybrid imaging. One board certified body radiologists and a nuclear medicine specialist performed a consensus reading of the whole-body PET/MRI sequences (Table 4). Comparable to the MRI datasets, two suspicious lesions with pathologic SUVs were detected. Further diagnostic work-up revealed the correct identification of one patient with rectal cancer and one false positive diagnosis (inflammatory subcutaneous lesion versus tumorous).

Diagnostic confidence. Diagnostic confidence for whole-body staging reached higher values for hybrid PET/MRI with 4.8 when compared to sole MRI with 4.5.

Table 4. Results of whole-body PET/MRI.

Patient #	Whole-body MRI	Whole-body PET	Whole-body diagnosis
1	-	-	
2	-	-	
3	+	+	rectal cancer
4	-	-	
5	-	-	
6	-	-	
7	-	-	
8	-	-	
9	-	-	
10	-	-	
11	-	-	
12	-	-	
13	-	-	
14	+	+	false positive
15	-	-	
16	-	-	
17	-	-	
18	-	-	
19	-	-	
20	-	-	

https://doi.org/10.1371/journal.pone.0227906.t004

Discussion

Our study results on ^{18}F-FDG PET/MRI in the diagnostic work-up of limbic encephalitis deliver three important findings: First, hybrid ^{18}F-FDG-PET/MRI identified more patients with LE compared to MRI alone. Second, hybrid ^{18}F-FDG-PET/MRI scored higher diagnostic confidence to identify LE compared to MRI alone. Overall, both aspects underline the importance and additional diagnostic value of ^{18}F-FDG to MRI, providing complementary information for an improved diagnosis of LE patients.

LE experienced growing recognition within the last years as a rare cause of altered mental status [17, 18]. Diagnosis is often missed or delayed due to an unspecific clinical presentation with limbic dysfunction as the single most consistent finding [19]. Diagnosis of LE is based on imaging in addition to clinical presentation with limbic symptoms, specific antibody subtypes and EEG patterns [9]. Imaging of LE is mainly based on MRI and analysis of FLAIR and T2-w images, commonly comprising volume alterations and swelling-induced signal increase on T2-w and FLAIR images of the limbic system [2, 3, 14, 20]. Nevertheless, a variety of imaging findings have been reported for extra-limbic areas, including the frontal or parietal cortices [21–24], the cerebellum or the brain stem [8, 25, 26]. Showing a great variety of occurrence of pathological findings in MRI, ranging from less than 10% to 100% [8, 23], MRI has been demonstrated to yield false negative results in a vast number of patients [2]. While no direct correlation to influencing factors has been identified that could explain these highly variable imaging findings, there seems to be an association to specific subtypes such as the group of II anti-N-methyl-D-aspartate (NMDA) receptor and VGKC (Voltage-gated potassium channel)-associated encephalitis [2, 27, 28].

In addition to cerebral MRI whole-body ^{18}F-FDG-PET is often performed for tumor screening in LE patients to rule out paraneoplastic limbic encephalitis and has been shown to

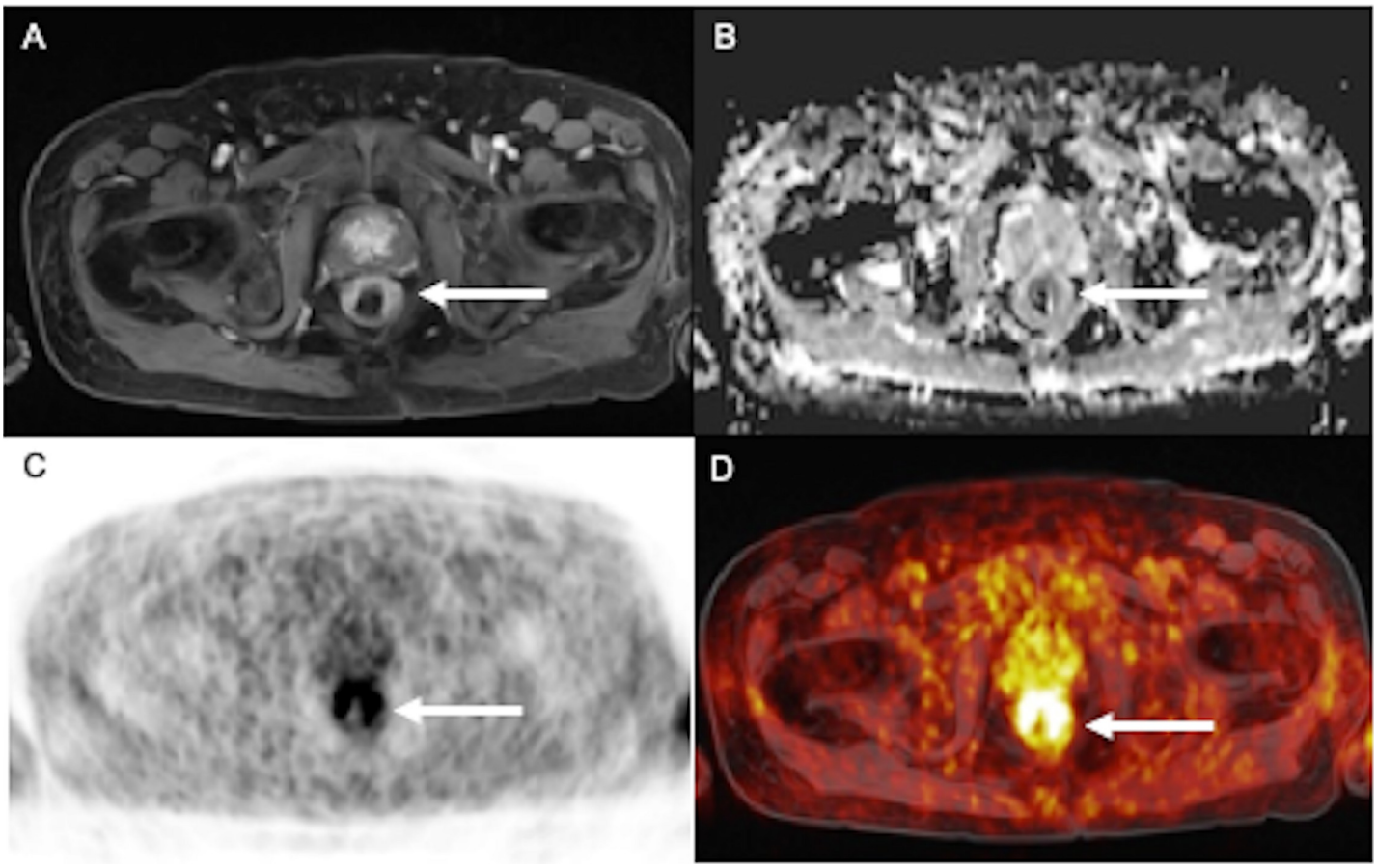

Fig 3. 75-year old patient with circumscribed thickening of the rectal wall and dull contrast enhancement (A), with a distinct diffusion restriction on the ADC-MAP (B). PET shows an intense semicircular tracer uptake with SUVmax of 8.8 (C, D). Final histopathological diagnosis was a rectal cancer.

https://doi.org/10.1371/journal.pone.0227906.g003

be highly sensitive for the detection of epileptogenic lesions [29, 30] and may also support the diagnosis of LE. To date, most ^{18}F-FDG-PET publications describe changes in the mesial temporal metabolism, often accompanied by a variety of further metabolic changes in the associating cortex as well as relative metabolic sparing of primary cortices, cerebellum and striatum [8, 31–34]. Nevertheless, comparable to the wide range of variable changes in MRI, ^{18}F-FDG-PET has also been reported to yield varying metabolic changes from hyper- and hypometabolism involving various regions of the brain to completely normal ^{18}F-FDG-PET scans [8, 31, 35]. A number of studies indicate that these PET findings (in the limbic system and extra-limbic regions) were associated with clinical symptoms and active disease status more strongly than the MRI findings [7, 36]. A recent Editorial emphasized the importance of harmonized brain ^{18}F-FDG-PET protocols, making PET findings consistent and comparable between different centers [37]. Combining the strength of both MRI and PET in a single temporal as well as spatial domain, as well as facilitating a one-stop-shop examination, by means of cerebral and whole-body imaging, the aim of our study was to investigate the according morphologic and metabolic changes in patients with LE while ruling out potential causes for paraneoplastic limbic encephalitis. To date, most studies on hybrid imaging in LE put the focus on the sole investigation of PET or MRI, with only a few case reports describing the utilization of integrated PET/MRI for LE diagnostics [38]. Our results confirm previous studies in demonstrating a great variety of morphologic and metabolic changes in patients with LE in the limbic system

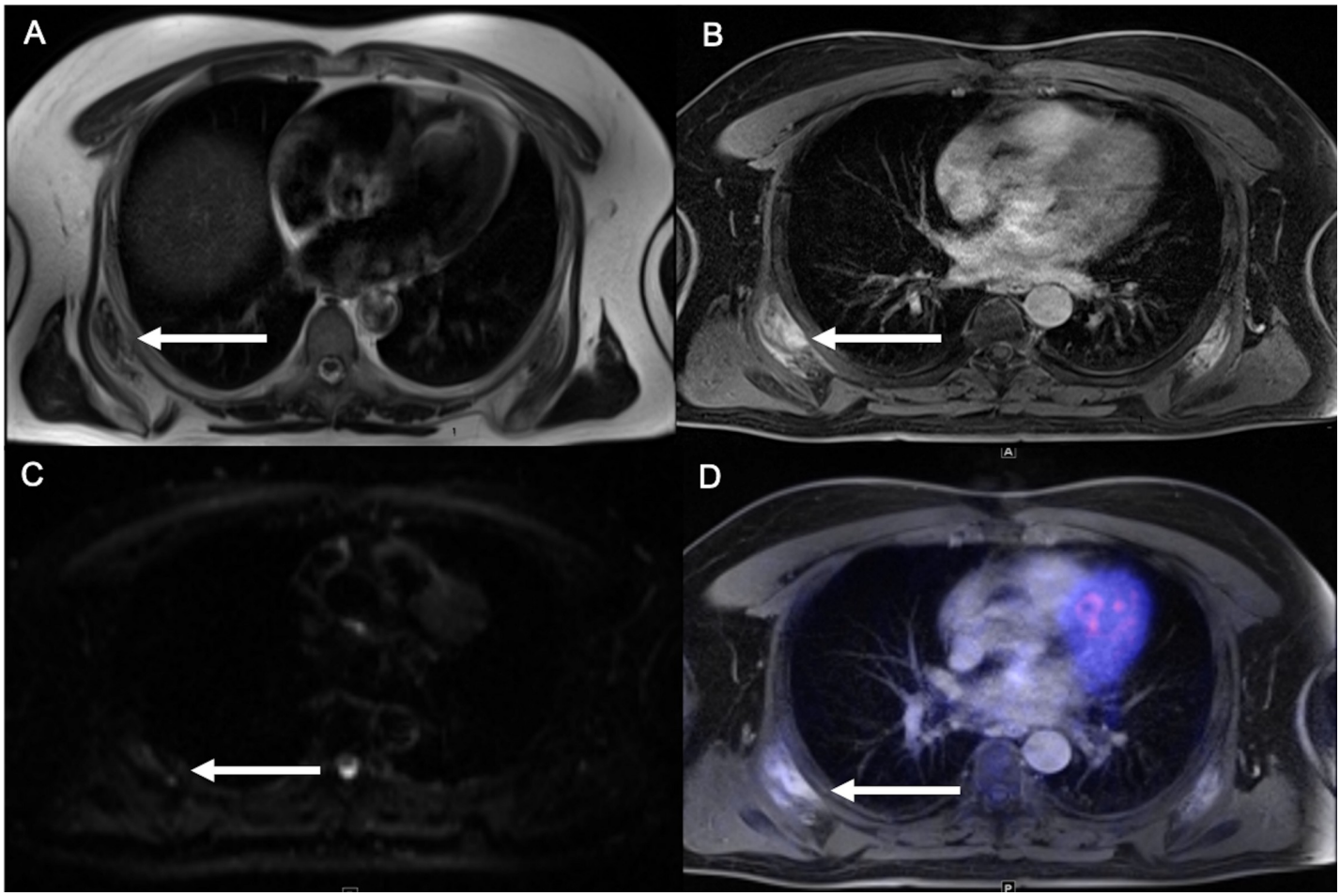

Fig 4. 59-year old patient with suspicious subscapular lesions with isointense signal on T2w (A), intense inhomogeneous contrast enhancement (B), no diffusion restriction (C) and mild tracer uptake with SUVmax of 3.2 (D).

https://doi.org/10.1371/journal.pone.0227906.g004

and extra limbic areas as well as the importance and great diagnostic value of adding ^{18}F-FDG-PET to the morphologic assessment. Overall, MRI showed high diagnostic accuracy for the correct identification of LE with 16/20 patients. PET was negative in 9 of these patients, and positive in metabolic changes of the limbic system and/or extra limbic areas in 7 patients underlining the previously published variability of involved brain regions (Table 3). These results go inline with observations by Probasco et al. suggesting that autoimmune encephalitis may involve broader metabolic abnormalities detectable by ^{18}F-FDG-PET in extra limbic areas of the brain [39]. In accordance with previous publications, the vast majority of patients showed hypometabolism in our study with only one patient showing hypermetabolism of the limbic system (Table 3) [8, 40]. Apart from improving the diagnostic confidence, the added PET data also helped to correctly identify patients with negative MRI, in revealing metabolic changes of the limbic system in two patients and of the extra limbic system in one more patient. Overall, the results of our study and previous publications indicate that ^{18}F-FDG-PET may facilitate complementary information to morphologic MR features and may represent a sensitive and early biomarker for LE [39]. Nevertheless, the rather low scoring rates of diagnostic confidence of brain PET/MRI for detection of LE when compared to body PET/MRI clearly illustrate the remaining and outstandingly high challenges of imaging based LE diagnosis.

Apart from facilitating the dual assessment of cerebral morphologic and metabolic data, integrated PET/MRI also enables dual assessment of cerebral and whole-body imaging. With tumor-induced paraneoplastic limbic encephalitis being one of the three major causes of limbic encephalitis, patients suspected of LE commonly undergo whole-body imaging to rule out underlying oncologic diseases. As reported in a vast amount of previous publications integrated PET/MRI facilitates a highly valuable platform for whole-body staging [15, 41–43]. In our study, an underlying oncologic disease could be ruled out in 18 patients, while one patient with rectal cancer could be correctly identified, and one suspicious subcutaneous lesion in another patient was false positive in MRI as well as PET.

Overall, our study is not free of limitations. The clinical setting of the study resulted in the inclusion of a heterogeneous cohort of a minority of treated and majority of untreated patients. Although no direct interdependency between treatment and PET/MRI analysis can be concluded, this issue of heterogeneity and the small patient cohort should be addressed in future trials comprising larger patient cohorts.

Overall, our study results underline the importance and diagnostic value of the combined morphologic and metabolic assessment for LE diagnostics. Furthermore, they demonstrate the manifold benefit of integrated PET/MRI systems in facilitating not only a simultaneous analysis of MRI and PET, but also of cerebral and whole-body data.

Author Contributions

Conceptualization: Theodor Rüber, Michael Forsting, Christian E. Elger, Lale Umutlu.

Data curation: Theodor Rüber, Leon Ernst.

Formal analysis: Cornelius Deuschl, Wolfgang P. Fendler, Christoph Mönninghoff, Lale Umutlu.

Investigation: Cornelius Deuschl, Christoph Mönninghoff, Lale Umutlu.

Methodology: Ken Herrmann, Lale Umutlu.

Project administration: Cornelius Deuschl, Theodor Rüber, Julian Kirchner.

Resources: Christian E. Elger.

Supervision: Lale Umutlu.

Validation: Lale Umutlu.

Visualization: Cornelius Deuschl.

Writing – original draft: Cornelius Deuschl, Lale Umutlu.

Writing – review & editing: Theodor Rüber, Wolfgang P. Fendler, Ken Herrmann, Carlos M. Quesada, Michael Forsting, Lale Umutlu.

References

1. Oyanguren B, Sanchez V, Gonzalez FJ, de Felipe A, Esteban L, Lopez-Sendon JL, et al. Limbic encephalitis: a clinical-radiological comparison between herpetic and autoimmune etiologies. Eur J Neurol. 2013; 20(12):1566–70. Epub 2013/08/15. https://doi.org/10.1111/ene.12249 PMID: 23941332.
2. Wagner J, Schoene-Bake JC, Malter MP, Urbach H, Huppertz HJ, Elger CE, et al. Quantitative FLAIR analysis indicates predominant affection of the amygdala in antibody-associated limbic encephalitis. Epilepsia. 2013; 54(9):1679–87. Epub 2013/07/31. https://doi.org/10.1111/epi.12320 PMID: 23889589.
3. Wagner J, Witt JA, Helmstaedter C, Malter MP, Weber B, Elger CE. Automated volumetry of the mesiotemporal structures in antibody-associated limbic encephalitis. J Neurol Neurosurg Psychiatry. 2015; 86(7):735–42. Epub 2014/09/04. https://doi.org/10.1136/jnnp-2014-307875 PMID: 25185210.

4. Urbach H, Rauer S, Mader I, Paus S, Wagner J, Malter MP, et al. Supratentorial white matter blurring associated with voltage-gated potassium channel-complex limbic encephalitis. Neuroradiology. 2015; 57(12):1203–9. Epub 2015/08/22. https://doi.org/10.1007/s00234-015-1581-x PMID: 26293130.
5. Wagner J, Schoene-Bake JC, Witt JA, Helmstaedter C, Malter MP, Stoecker W, et al. Distinct white matter integrity in glutamic acid decarboxylase and voltage-gated potassium channel-complex antibody-associated limbic encephalitis. Epilepsia. 2016; 57(3):475–83. Epub 2016/01/11. https://doi.org/10.1111/epi.13297 PMID: 26749370.
6. Scheid R, Lincke T, Voltz R, von Cramon DY, Sabri O. Serial 18F-fluoro-2-deoxy-D-glucose positron emission tomography and magnetic resonance imaging of paraneoplastic limbic encephalitis. Arch Neurol. 2004; 61(11):1785–9. Epub 2004/11/10. https://doi.org/10.1001/archneur.61.11.1785 PMID: 15534190.
7. Ances BM, Vitaliani R, Taylor RA, Liebeskind DS, Voloschin A, Houghton DJ, et al. Treatment-responsive limbic encephalitis identified by neuropil antibodies: MRI and PET correlates. Brain. 2005; 128(Pt 8):1764–77. Epub 2005/05/13. https://doi.org/10.1093/brain/awh526 PMID: 15888538; PubMed Central PMCID: PMC1939694.
8. Baumgartner A, Rauer S, Mader I, Meyer PT. Cerebral FDG-PET and MRI findings in autoimmune limbic encephalitis: correlation with autoantibody types. Journal of neurology. 2013; 260(11):2744–53. Epub 2013/08/01. https://doi.org/10.1007/s00415-013-7048-2 PMID: 23900756.
9. Bien CG DGfrN. Immunvermittelte Erkrankungen der grauen ZNS Substanz sowie Neurosarkoidose. https://wwwdgnorg/leitlinien/2396-ll-32-.2012;accessed 10/4/2018(Deutsche Gesellschaft für Neurologie).
10. Graus F, Titulaer MJ, Balu R, Benseler S, Bien CG, Cellucci T, et al. A clinical approach to diagnosis of autoimmune encephalitis. Lancet Neurol. 2016; 15(4):391–404. Epub 2016/02/26. https://doi.org/10.1016/S1474-4422(15)00401-9 PMID: 26906964; PubMed Central PMCID: PMC5066574.
11. Varrone A, Asenbaum S, Vander Borght T, Booij J, Nobili F, Nagren K, et al. EANM procedure guidelines for PET brain imaging using [18F]FDG, version 2. Eur J Nucl Med Mol Imaging. 2009; 36(12):2103–10. Epub 2009/10/20. https://doi.org/10.1007/s00259-009-1264-0 PMID: 19838705.
12. van Swieten JC, Koudstaal PJ, Visser MC, Schouten HJ, van Gijn J. Interobserver agreement for the assessment of handicap in stroke patients. Stroke. 1988; 19(5):604–7. https://doi.org/10.1161/01.str.19.5.604 PMID: 3363593.
13. Quick HH. Integrated PET/MR. Journal of magnetic resonance imaging: JMRI. 2014; 39(2):243–58. Epub 2013/12/18. https://doi.org/10.1002/jmri.24523 PMID: 24338921.
14. Urbach H, Soeder BM, Jeub M, Klockgether T, Meyer B, Bien CG. Serial MRI of limbic encephalitis. Neuroradiology. 2006; 48(6):380–6. Epub 2006/04/06. https://doi.org/10.1007/s00234-006-0069-0 PMID: 16586118.
15. Grueneisen J, Beiderwellen K, Heusch P, Gratz M, Schulze-Hagen A, Heubner M, et al. Simultaneous positron emission tomography/magnetic resonance imaging for whole-body staging in patients with recurrent gynecological malignancies of the pelvis: a comparison to whole-body magnetic resonance imaging alone. Investigative radiology. 2014; 49(12):808–15. Epub 2014/07/11. https://doi.org/10.1097/RLI.0000000000000086 PMID: 25010207.
16. Erhamamci S, Reyhan M, Nursal GN, Torun N, Yapar AF, Findikcioglu A, et al. Elastofibroma dorsi incidentally detected by (18)F-FDG PET/CT imaging. Ann Nucl Med. 2015; 29(5):420–5. Epub 2015/02/11. https://doi.org/10.1007/s12149-015-0959-5 PMID: 25666569.
17. Degnan AJ, Levy LM. Neuroimaging of rapidly progressive dementias, part 2: prion, inflammatory, neoplastic, and other etiologies. AJNR American journal of neuroradiology. 2014; 35(3):424–31. Epub 2013/02/16. https://doi.org/10.3174/ajnr.A3455 PMID: 23413251.
18. Degnan AJ, Levy LM. Neuroimaging of rapidly progressive dementias, part 1: neurodegenerative etiologies. AJNR American journal of neuroradiology. 2014; 35(3):418–23. Epub 2013/02/26. https://doi.org/10.3174/ajnr.A3454 PMID: 23436051.
19. Lancaster E, Lai M, Peng X, Hughes E, Constantinescu R, Raizer J, et al. Antibodies to the GABA(B) receptor in limbic encephalitis with seizures: case series and characterisation of the antigen. Lancet Neurol. 2010; 9(1):67–76. Epub 2009/12/08. https://doi.org/10.1016/S1474-4422(09)70324-2 PMID: 19962348; PubMed Central PMCID: PMC2824142.
20. Schievelkamp AH, Jurcoane A, Ruber T, Ernst L, Muller A, Madler B, et al. Limbic Encephalitis in Patients with Epilepsy-is Quantitative MRI Diagnostic? Clin Neuroradiol. 2018. Epub 2018/07/18. https://doi.org/10.1007/s00062-018-0705-1 PMID: 30014154.
21. Greiner H, Leach JL, Lee KH, Krueger DA. Anti-NMDA receptor encephalitis presenting with imaging findings and clinical features mimicking Rasmussen syndrome. Seizure. 2011; 20(3):266–70. Epub 2010/12/15. https://doi.org/10.1016/j.seizure.2010.11.013 PMID: 21146427.

22. Pillai SC, Gill D, Webster R, Howman-Giles R, Dale RC. Cortical hypometabolism demonstrated by PET in relapsing NMDA receptor encephalitis. Pediatr Neurol. 2010; 43(3):217–20. Epub 2010/08/10. https://doi.org/10.1016/j.pediatrneurol.2010.04.019 PMID: 20691947.

23. Gultekin SH, Rosenfeld MR, Voltz R, Eichen J, Posner JB, Dalmau J. Paraneoplastic limbic encephalitis: neurological symptoms, immunological findings and tumour association in 50 patients. Brain. 2000; 123 (Pt 7):1481–94. Epub 2000/06/27. https://doi.org/10.1093/brain/123.7.1481 PMID: 10869059.

24. Pruss H, Dalmau J, Harms L, Holtje M, Ahnert-Hilger G, Borowski K, et al. Retrospective analysis of NMDA receptor antibodies in encephalitis of unknown origin. Neurology. 2010; 75(19):1735–9. Epub 2010/11/10. https://doi.org/10.1212/WNL.0b013e3181fc2a06 PMID: 21060097.

25. Dalmau J, Tuzun E, Wu HY, Masjuan J, Rossi JE, Voloschin A, et al. Paraneoplastic anti-N-methyl-D-aspartate receptor encephalitis associated with ovarian teratoma. Ann Neurol. 2007; 61(1):25–36. Epub 2007/01/31. https://doi.org/10.1002/ana.21050 PMID: 17262855; PubMed Central PMCID: PMC2430743.

26. Cistaro A, Caobelli F, Quartuccio N, Fania P, Pagani M. Uncommon 18F-FDG-PET/CT findings in patients affected by limbic encephalitis: hyper-hypometabolic pattern with double antibody positivity and migrating foci of hypermetabolism. Clin Imaging. 2015; 39(2):329–33. Epub 2014/12/10. https://doi.org/10.1016/j.clinimag.2014.09.004 PMID: 25487436.

27. Florance NR, Davis RL, Lam C, Szperka C, Zhou L, Ahmad S, et al. Anti-N-methyl-D-aspartate receptor (NMDAR) encephalitis in children and adolescents. Ann Neurol. 2009; 66(1):11–8. Epub 2009/08/12. https://doi.org/10.1002/ana.21756 PMID: 19670433; PubMed Central PMCID: PMC2826225.

28. Irani SR, Bera K, Waters P, Zuliani L, Maxwell S, Zandi MS, et al. N-methyl-D-aspartate antibody encephalitis: temporal progression of clinical and paraclinical observations in a predominantly non-paraneoplastic disorder of both sexes. Brain. 2010; 133(Pt 6):1655–67. Epub 2010/06/01. https://doi.org/10.1093/brain/awq113 PMID: 20511282; PubMed Central PMCID: PMC2877907.

29. Chassoux F, Rodrigo S, Semah F, Beuvon F, Landre E, Devaux B, et al. FDG-PET improves surgical outcome in negative MRI Taylor-type focal cortical dysplasias. Neurology. 2010; 75(24):2168–75. Epub 2010/12/22. https://doi.org/10.1212/WNL.0b013e31820203a9 PMID: 21172840.

30. Rubi S, Setoain X, Donaire A, Bargallo N, Sanmarti F, Carreno M, et al. Validation of FDG-PET/MRI coregistration in nonlesional refractory childhood epilepsy. Epilepsia. 2011; 52(12):2216–24. Epub 2011/11/05. https://doi.org/10.1111/j.1528-1167.2011.03295.x PMID: 22050207.

31. Vitaliani R, Mason W, Ances B, Zwerdling T, Jiang Z, Dalmau J. Paraneoplastic encephalitis, psychiatric symptoms, and hypoventilation in ovarian teratoma. Ann Neurol. 2005; 58(4):594–604. Epub 2005/09/24. https://doi.org/10.1002/ana.20614 PMID: 16178029; PubMed Central PMCID: PMC2245881.

32. Mohr BC, Minoshima S. F-18 fluorodeoxyglucose PET/CT findings in a case of anti-NMDA receptor encephalitis. Clin Nucl Med. 2010; 35(6):461–3. Epub 2010/05/19. https://doi.org/10.1097/RLU.0b013e3181db4d4a PMID: 20479604.

33. Rey C, Koric L, Guedj E, Felician O, Kaphan E, Boucraut J, et al. Striatal hypermetabolism in limbic encephalitis. Journal of neurology. 2012; 259(6):1106–10. Epub 2011/11/15. https://doi.org/10.1007/s00415-011-6308-2 PMID: 22081102.

34. Leypoldt F, Buchert R, Kleiter I, Marienhagen J, Gelderblom M, Magnus T, et al. Fluorodeoxyglucose positron emission tomography in anti-N-methyl-D-aspartate receptor encephalitis: distinct pattern of disease. J Neurol Neurosurg Psychiatry. 2012; 83(7):681–6. Epub 2012/05/09. https://doi.org/10.1136/jnnp-2011-301969 PMID: 22566598; PubMed Central PMCID: PMC3740122.

35. Kassubek J, Juengling FD, Nitzsche EU, Lucking CH. Limbic encephalitis investigated by 18FDG-PET and 3D MRI. J Neuroimaging. 2001; 11(1):55–9. Epub 2001/02/24. https://doi.org/10.1111/j.1552-6569.2001.tb00011.x PMID: 11198529.

36. Morbelli S, Djekidel M, Hesse S, Pagani M, Barthel H, Neuroimaging Committee of the European Association of Nuclear M, et al. Role of (18)F-FDG-PET imaging in the diagnosis of autoimmune encephalitis. Lancet Neurol. 2016; 15(10):1009–10. Epub 2016/08/30. https://doi.org/10.1016/S1474-4422(16)30140-5 PMID: 27571149.

37. Morbelli S, Arbizu J, Booij J, Chen MK, Chetelat G, Cross DJ, et al. The need of standardization and of large clinical studies in an emerging indication of [(18)F]FDG PET: the autoimmune encephalitis. Eur J Nucl Med Mol Imaging. 2017; 44(3):353–7. Epub 2016/12/08. https://doi.org/10.1007/s00259-016-3589-9 PMID: 27924371.

38. Taneja S, Suri V, Ahuja A, Jena A. Simultaneous 18F- FDG PET/MRI in Autoimmune Limbic Encephalitis. Indian J Nucl Med. 2018; 33(2):174–6. Epub 2018/04/13. https://doi.org/10.4103/ijnm.IJNM_147_17 PMID: 29643688; PubMed Central PMCID: PMC5883445.

39. Probasco JC, Solnes L, Nalluri A, Cohen J, Jones KM, Zan E, et al. Abnormal brain metabolism on FDG-PET/CT is a common early finding in autoimmune encephalitis. Neurol Neuroimmunol

Neuroinflamm. 2017; 4(4):e352. Epub 2017/06/02. https://doi.org/10.1212/NXI.0000000000000352 PMID: 28567435; PubMed Central PMCID: PMC5442608.

40. Fisher RE, Patel NR, Lai EC, Schulz PE. Two different 18F-FDG brain PET metabolic patterns in autoimmune limbic encephalitis. Clin Nucl Med. 2012; 37(9):e213–8. Epub 2012/08/15. https://doi.org/10.1097/RLU.0b013e31824852c7 PMID: 22889795.

41. Beiderwellen K, Grueneisen J, Ruhlmann V, Buderath P, Aktas B, Heusch P, et al. [(18)F]FDG PET/MRI vs. PET/CT for whole-body staging in patients with recurrent malignancies of the female pelvis: initial results. Eur J Nucl Med Mol Imaging. 2015; 42(1):56–65. Epub 2014/09/17. https://doi.org/10.1007/s00259-014-2902-8 PMID: 25223420.

42. Grueneisen J, Sawicki LM, Schaarschmidt BM, Suntharalingam S, von der Ropp S, Wetter A, et al. Evaluation of a Fast Protocol for Staging Lymphoma Patients with Integrated PET/MRI. PLoS One. 2016; 11(6):e0157880. Epub 2016/06/22. https://doi.org/10.1371/journal.pone.0157880 PMID: 27327617; PubMed Central PMCID: PMC4915683.

43. Kirchner J, Grueneisen J, Martin O, Oehmigen M, Quick HH, Bittner AK, et al. Local and whole-body staging in patients with primary breast cancer: a comparison of one-step to two-step staging utilizing (18)F-FDG-PET/MRI. Eur J Nucl Med Mol Imaging. 2018; 45(13):2328–37. Epub 2018/07/30. https://doi.org/10.1007/s00259-018-4102-4 PMID: 30056547.

DOI: 10.1371/journal.pone.0227906
URN: urn:nbn:de:hbz:464-20200605-115027-6